REPORT DOCUMENTATION PAGE

Form Approved OMB No. 0704-0188

1. REPORT DATE *(DD-MM-YYYY)*	2. REPORT TYPE	3. DATES COVERED *(From – To)*
	Final Report	13 November 2008 - 13-Nov-09

4. TITLE AND SUBTITLE

Quantifying light manipulation in marine diatoms

5a. CONTRACT NUMBER
FA8655-09-1-3018

5b. GRANT NUMBER

5c. PROGRAM ELEMENT NUMBER

6. AUTHOR(S)

Dr. Peter Vukusic

5d. PROJECT NUMBER

5d. TASK NUMBER

5e. WORK UNIT NUMBER

7. PERFORMING ORGANIZATION NAME(S) AND ADDRESS(ES)

University of Exeter
Stocker Road
Exeter EX4 4QL
United Kingdom

8. PERFORMING ORGANIZATION REPORT NUMBER

N/A

9. SPONSORING/MONITORING AGENCY NAME(S) AND ADDRESS(ES)

EOARD
Unit 4515 BOX 14
APO AE 09421

10. SPONSOR/MONITOR'S ACRONYM(S)

11. SPONSOR/MONITOR'S REPORT NUMBER(S)
Grant 09-3018

12. DISTRIBUTION/AVAILABILITY STATEMENT

Approved for public release; distribution is unlimited.

13. SUPPLEMENTARY NOTES

14. ABSTRACT

This report results from a contract tasking University of Exeter as follows: Our investigation will comprise five principle sections:
1. Determination of the ranges and geometries of the most common forms of diatom structures.
This will enable selection of representative species for optical characterisation and will be accomplished thorough literature searches and short visits to two eminent diatom biology specialists (in Germany and in Belgium).
2. Measurement of absolute spectral transmittance of diatom valve structures
Experimental analysis will be challenging due to the microscopic sizes of individual diatoms and the difficulty with which conventional optical experiments may be applied to the study of constituent parts of isolated individual diatoms. To this end, we aim to refine the process that was originally developed to characterise optically the isolated single photonic scales of butterflies, applying it in turn both to single whole diatoms and also to individual separated valves.
3. Rigourous SEM and TEM analysis of diatom valve ultrastructures.
This will yield ultrastructure symmetry geometries and periodicity-dimensions with which light interaction may be modeled. The resulting theoretical band diagrams and calculated diffraction efficiencies will be compared and contrasted to experimental data.
4. Finite-element based computer modelling.
Comsol (formerly Femlab) will be used to recreate virtual 3D diatom structures and model light interaction.
5. Measurement of the spatial symmetry of diffractive interaction of incident light with diatom ultrastructures.
This will offer insight into the key assumed potential advantages associated with diatom ultrastructure evolution. Additionally, it will offer strong indication of the feasibility of incorporating natural and also cell-cultured and mineral- or metal-infused diatoms into electro-optical devices.

15. SUBJECT TERMS
EOARD, Photonics, Bioinspired Design, biotemplate

16. SECURITY CLASSIFICATION OF:			17. LIMITATION OF ABSTRACT	18, NUMBER OF PAGES	19a. NAME OF RESPONSIBLE PERSON
a. REPORT	b. ABSTRACT	c. THIS PAGE			WYNN SANDERS, Maj, USAF
UNCLAS	UNCLAS	UNCLAS	UL	14	19b. TELEPHONE NUMBER *(Include area code)* +44 (0)1895 616 007

End of Project Summary Report

Investigation of Light Manipulation by the Ultrastructure of Marine Diatoms

Funded by the European Office of Aerospace Research & Development

Grant FA8855-09-1-3018

Value of award: $25,000

EOARD Contact: **Wynn Sanders**

Prof. Pete Vukusic

School of Physics, University of Exeter, Exeter EX4 4QL, UK

P.Vukusic@ex.ac.uk

Project Summary

Diatoms are well-known for the intricately patterned nanostructure of their silica-based cell walls. To date, the optical properties of diatom cell-wall ultrastructures have largely gone uncharacterised experimentally. The aim of this project comprised forming a detailed understanding of the way in which light interacts with the ultrastructure of a representative centric diatom species, *Coscinodiscus wailesii*, through both experimental investigation and theoretical modelling.

In the experimental component of this project, light interaction both with individual valves and whole bivalves of the diatom *C. wailesii* was measured. The results of these measurements were sufficiently novel and scientifically interesting for publication in Journal of Materials Science (*J. Mat. Res*. **23**, 3229 2009). This report represents a summary of the published data, subsequent analysis and detailed discussion.

The experimental optical characterisation of *C. wailesii* diatom frustules led to the observation of significant 6-fold symmetric diffraction through the valve ultrastructure. The efficiencies associated with this transmission were quantified to efficiencies that were strongly wavelength-dependent; approximately 80 % for red, 30% for green and 20% for blue light.

The associated detailed modelling of *C. wailesii* frustules structures was undertaken using the finite-element method. Initial theoretical results were collected just prior to the end of the project. These were not published but are presented in this report.

While these experimental results and conclusions based on their analysis may potentially offer insight into the role of periodic nanostructure in diatom selection, they are deemed important for consideration in the design of biomimetic optics-based diatom applications.

I. Introduction.

As biological entities, diatoms are ubiquitously present in nearly all aquatic environments on earth. They are eukaryotic algal organisms that comprise only one cell, that are photosynthetic and that have a long scientific history of study, partly due to the astonishingly intricate design and architecture of their silica-based cell walls[1].

Recently there has been increasing interest surrounding the exploitation of marine phytoplankta, principally diatoms, for use in a range of technological applications [1-3]. There are three principle reasons for this. The first is their species-related range of shapes, sizes and cell-wall nanopatterning[3]. For given specimens, this potentially offers a large range of available internal volume, of mechanical and optical properties, and of diffusion of material through the pores in their cell walls[4]. The second reason is the way in which diatoms may be influenced to biomineralise a range of materials[5,6] or to be used as templates for the fabrication of nanopatterned structures made of other materials such as silicon[7]. Thirdly, the chemistry of their surfaces may be modified so that they may be appended with biologically active components[8]. In one or more of these ways, processes of biofunctionalisation may transform collections of ordinary diatoms into finely tuned potential micro-devices and technological components[1,2,4].

The fabrication of designer diatom morphologies and surface biochemistries that are appropriate for use in a range of applications is a fascinating research goal. The manufacturing techniques for this endeavour have been progressing rapidly[9]. They include: cell-culture and genetic engineering mediated biofunctionalisation of diatom silicification processes[2]; controlled pore-size modification by atomic layer deposition of metal and semiconductor oxides[10], and also chemothermic reduction processes[7]. Structurally modified or unmodified diatom surfaces may also be manipulated for surface biochemistry applications associated with DNA, enzymes or immunoassays[8,10].

The biogenesis of diatom cell walls, the patterns on and in which are highly species specific, can be explained by molecular self-assembly[11] and phase-separation processes[12] that induce seawater-dissolved silicic acid to form highly geometric nanopatterns. The size and spacing of the nanopores may be affected by organic components such as silaffins and polyamines which are known to govern silica precipitation[12].

For several potential applications, the way in which diatom ultrastructures interact with light is of primary concern. If, for example, light sensitive fluorophores were housed inside diatoms[4] for a specific application, then knowledge of the efficiency and manner in which light could couple into and out from those fluorophores would be essential. Additionally, if, through cell-culture assembly processes, electroluminescent (EL) semiconductor material was incorporated into diatom species[5], the inherent optical properties of the nanopatterned diatom structure would need to be known if the added effect of the semiconductor EL emission is to be identified or its function optimised.

In other biological organisms, such as insecta, nanopatterned ultrastructures comprising periodic or quasi-periodic spatial variations in refractive index, give rise to strong photonic effects. These effects are well documented across a broad range of species through many detailed optical studies[13-15]. A number of them have gone on to inspire specific biomimetic applications[16-17]. The nature and true extent of diatoms' photonic character, however, has so far been unavailable through optical experiments. We believe such experiments would primarily provide practical evidence for consideration in the development of diatom-related optics based technological applications[4]. Furthermore, since such light manipulation in diatoms is experimentally undetermined, its significance in the biological selection and development of diatom ultrastructure is unclear. The possible optical role played by this ultrastructure is intriguing. Not only do the dimensions and geometries of diatom cell wall nanopatterning suggest they should produce strong interaction with light of visible wavelengths[18] but theoretical modelling carried out on simplified diatom models[19] also points to light manipulation capability. Certainly, any manipulation of light by diatoms' ultrastructures is of fundamental biological importance since it would affect the light environment in their interiors. This would in turn control the optical conditions for light harvesting by the biological antennas of their chloroplasts that collect energy from large absorption cross-sections and direct it to photosynthesis reaction centres[20]. Light manipulation by diatom valve ultrastructure should therefore be considered when assessing the variables involved in diatom success.

In this report, we present experimental data that reveal the nature of the interaction between incident light and the periodic ultrastructure of a representative centrally symmetric species of marine diatom, *Coscinodiscus wailesii*. We discuss the results in the context of technological applications and biological significance.

II. Materials and Methods.

A. Sample details

C.wailesii is typical of the largest diatom genus *Coscinodiscus* (Class *Bacillariophyceae*, order *Centrales*). It exhibits central symmetry like other *Centrales* phytoplankta and comprises intricately patterned cell walls that consist of amorphous silica[12]. Two overlapping valves (the thecae) with diameters in the range 200 – 350 μm, form its shell walls (frustules) (figure 1a). The shell walls, of thickness approximately 2.0 (± 0.1) μm, are themselves formed by two co-joined plates, one which is internal and the other external to the diatom. The outer plate is a thin silica layer comprising a complex hexagonal arrangement of hollow pores of typical approximate diameter 250 (± 20) nm and typical lattice constant 400 (± 50) nm. Similarly, the inner silica layer is

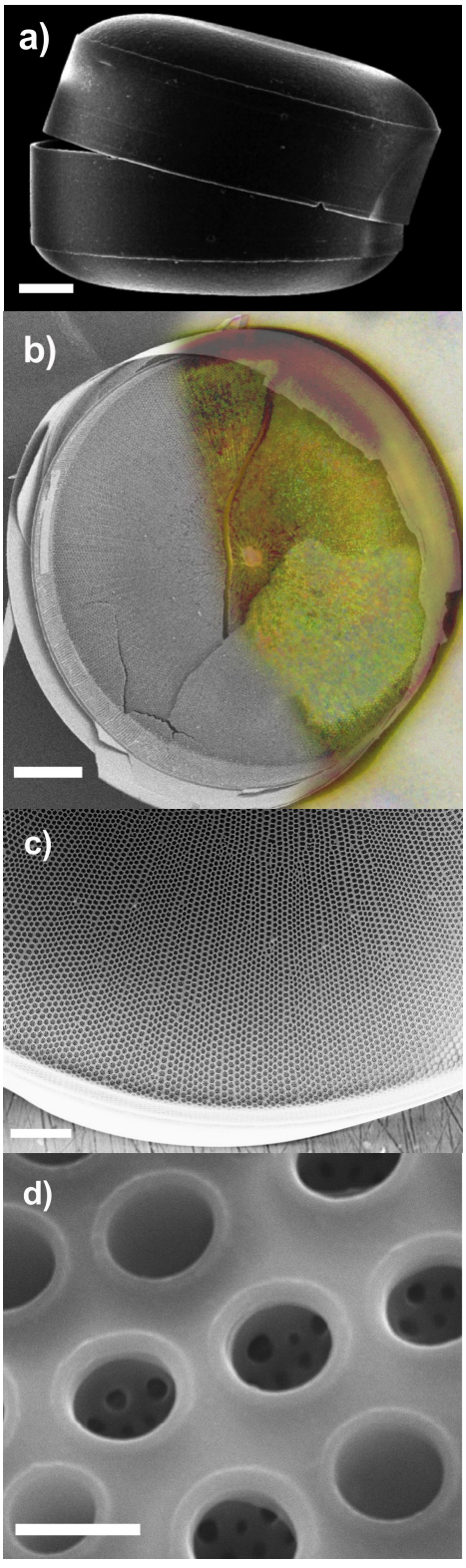

Figure 1. a) SEM image of two overlapping valves from a representative centric diatom; b) SEM image of the inner surface of a cleaned *C. wailesii* valve, partially superposed (on the right) with an optical image showing structural colour created by the valve's ultrastructure alone; c) and d) SEM images of the array of ultrastructure from a *C. wailesii* valve's internal surface (the smaller diameter holes from the valve outer surface that is arranged with smaller periodicity is visible (in d) through the larger diameter hole array). [Scale bars: a) and b) 50 μm; c) 20 μm; d) 1 μm].

perforated with hexagonally spaced pores; however, they are larger in scale with typical approximate diameter 1.3 (± 0.1) μm and typical lattice constant 2.0 (± 0.2) μm (figure 1b-d). Large numbers (ca. several hundred) of chlorophyll-rich organelles inhabit the interior space between the valves of living *C. wailesii* diatoms.

B. Sample preparation

The *C. wailesii* diatoms used in this study were obtained from a growing cell culture by treating the harvested cells twice with hot 2% SDS- 100 mM EDTA to remove intracellular material, membranes and wall coatings. The mixture was then separated using low-speed centrifugation (1000g), washed repeatedly with water, and dried following the method described in detail elsewhere[12].

C. Imaging

Individual diatoms and their separated valves were examined optically using a Carl Zeiss Axioskop 2 polarizing microscope and by electron microscopy using a Hitachi S-3200N scanning electron microscope (SEM). Prior to SEM imaging, samples were cold sputtered with 12 nm of chromium.

D. Optical data collection

The experimental methods with which single structurally coloured butterfly scales were previously characterised[21] were applied to the diatom characterisation in this study. In this way it was possible to characterise the wavelength, polarisation and angle-dependent photonic properties of needle-mounted diatom samples in significant detail. Single *C. wailesii* diatom valves and bivalves were mounted upright on individual ground-down needle tips. These were placed in turn at the centre of the optical path of a laser track while concurrently at the centre of an Euler cradle (normally used for holding, centering and orienting crystal samples during X-ray diffraction experiments). This permitted accurate micro-orienting of each single valve or bivalve with respect to the incident laser light. Each sample was measured in air and, with the supporting needle inverted, was immersed and measured in water.

The intensities and polarisations of the laser light sources were controlled using appropriate filters. Three lasers (with wavelengths 472 nm, 543 nm and 633 nm) were separately used to illuminate a 20 micrometer diameter area on the outer face of each diatom valve. Each laser was incident through a 1 kHz optical modulator that enabled phase sensitive detection and significantly improved signal quality[22]. A spatially apertured large-area photo-diode was angle-scanned around the sample in the horizontal plane for each incident laser, in both the reflection and transmission hemispheres. In this way the spatial form of the reflection and transmission from the diatom in this plane was collected[21]. The intensity of this reflection and transmission from the sample was then ratioed with the total light that was incident on the diatom which itself was quantified in the absence of the sample using the same collection method. This

permitted highly accurate calculation of the absolute proportion of light scattered in different directions as a result of interaction with the diatom's ultrastructure, a measurement which is often ineffectually performed using other methods[23].

To discern the spatial distribution of the light scattered from and through each sample, hemispherical screens were separately placed in front of and behind them. These screens allowed the intensity of this scattered light to be spatially sampled. The resulting screen-imaged spatial intensity distribution profiles were digitised and used, in conjunction with the calibrated angle-scan data from the same samples, to calculate the absolute proportion of power in any portion of reflected or transmitted solid angle.

Optical transmission data through the same samples were recorded when the laser sources were replaced with a single white light source. This illuminant was an Ocean Optics DH-2000-BAL source, brought to a 20 μm diameter focus with an F1.5 achromat. The wavelength-dependent transmission was collected using an Ocean Optics UV-Vis 400 μm diameter optical fibre connected to an Ocean Optics HR4000 high resolution UV-Vis-IR spectrometer and mounted on a mechanical arm whose rotation about the centrally placed sample was computer controlled.

III. Results

C. wailesii's nanopatterned valve ultrastructure diffracts light strongly both in air and in water. This was observed by optical microscopy; figure 1b shows the structurally coloured appearance of a cleaned single valve surface which occurs under suitable illumination when specific colours, which are complementary to the observed colour, are diffracted outside the microscope's objective lens collection angle. Early studies by Abbé noted this colour effect. It was attributed then, correctly, to diffraction from striae on diatoms' surfaces[24] and it has been used in certain instances with specially adapted microscope systems[25] for diatom taxonomy[26]. Such microscopy investigations that appear to show diatom structural colour provide very limited and incomplete information about the extent of light manipulation. More detailed analysis is essential. To this end, laser light was used to illuminate single needle-mounted diatom valves using the methods described earlier. Intense diffracted orders with 6-fold symmetry were observed (figure 2) both while they were held in air and also while immersed in water. Significantly less intense, but spatially analogous, diffraction was observed in reflection. The spatial distribution of this diffraction pattern, previously unobserved by early microscopy studies, is predictable from the 6-fold symmetry of the variation in refractive index of the valve ultrastructure, but is experimentally confirmed here for the first time. It may be verified by 2D fast Fourier transforms of the periodic ultrastructure of the internal surface geometry of the diatom which yield the same 6-fold momentum-space geometries as the diffraction patterns. Measurements of the angular separation of observed diffracted orders for each laser (e.g. 14.1 (± 0.5) ° for the 1st diffracted orders using 472 nm) further confirm that the 2 μm periodicity on the *C. wailesii* valve is the source of the observed diffraction. Some diffraction, albeit much less spatially regular, was also observed from whole cleaned bivalves.

In addition to facilitating strong diffractive effects, the valve ultrastructure creates a separate optical effect. The efficiency of transmission of light through the diatom valve, and therefore into the interior of the diatom, depends strongly on wavelength. This result was found to be largely independent of whether the surrounding medium was air or water. It was relatively low for blue and green wavelengths with mean absolute totals (measured using valves from five separate diatoms) of 22 (± 1) % for 472 nm incident light and 29 (± 1) % for 543 nm incident light. However, significantly higher absolute transmission, 78 (± 2) %, was measured for red light (633 nm). The mechanism for this differential colour transmission is caused by photonic interaction between the outer and inner valve wall. Theoretical band diagrams of simplified centric diatom ultrastructures[19] indicate the efficiency with which light is coupled into guided modes between the valve shell walls is strongly wavelength-dependent. This is manifested here experimentally as wavelength-dependent transmission. Very similar results were obtained for each of the valves measured from five separate *C. wailesii* diatoms when the laser sources were replaced with a white light source (figure 3). The diffraction described previously is also observed in this data; the zero diffracted order running vertically up the graph at the zero degrees (on the horizontal transmission angle axis), and two first diffracted orders running diagonally, one to the right and one to the left. This experimental diffraction data has been overlaid with theory generated using conservation of momentum in the normal way[27]; $k_s = k_0 + nk_g$, where k is the wavevector associated with the scattered light (s), the incident light (0), the periodicity of the valve surface (g), and where n takes integer values associated with the diffracted orders. The theoretically predicted diffraction follows both angle and wavelength features in the data very closely.

IV. Developing Theoretical Models.

The frustule of this diatom resembles a conventional photonic crystal slab, since the frustule itself is made up of two layers of amorphous silica, the outer, thicker layer pierced by a hexagonal array of holes, while the inner layer has a square array of smaller holes (figure 4). While the interaction of light with such a structure is measured experimentally in this investigation, it is equally important to understand the exact nature of the variables that control the interaction and which generate the resulting experimental observations. This task is undertaken using theoretical modelling. The protocols and methods with which the modeling was conducted here, is now described.

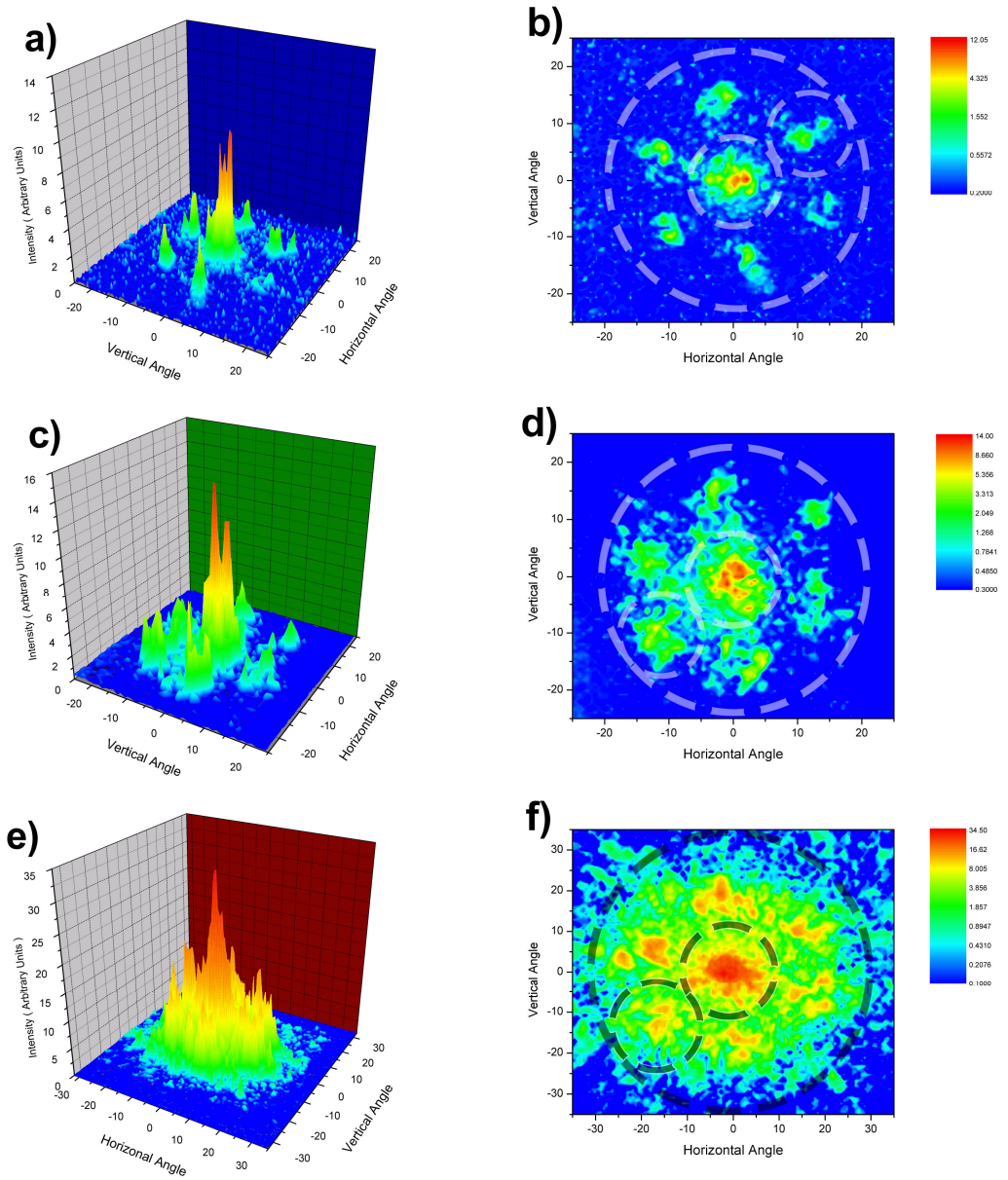

Figure 2: Graphs showing normalised representative experimental data signifying the spatial and intensity distributions of laser light (from 472 nm (graphs a) and b)), 543 nm (graphs c) and d)) and 633 nm (graphs e) and f)) lasers) transmitted through the same single valve of one *C. wailesii* diatom. Measured transmission efficiencies for each wavelength through this valve, associated with solid angle region represented by the hashed circles in figures b), d) and f) are as follows: b) 1.6 % [circled 1st order], 12.1 % [circled 0th order] and 21.6 % total transmission (large circle)]; d) 3.9 % [circled 1st order], 7.4 % [circled 0th order] and 29.7 % [total transmission (large circle)]; f) 8.9 % [circled 1st order], 26.8 % [circled 0th order] and 78.0 % [total transmission (large circle)].

A. Finite Element Modelling (FEM)

Finite Element Modelling allows complex numerical analysis of partial differential equations and integral equations along a path, across a surface or through a volume by dividing the length, area or volume into a number of discrete elements of finite size. This is known as discretisation, and is usually done by triangulation of the region, resulting in a triangular mesh.

For each element, numerical values are calculated at the nodes, then interpolated linearly along edges and throughout the enclosed volumes between the nodes. The error in the calculated values depends on the mesh density, with a dense mesh of small elements giving a closer approximation of the situation being modelled. In the hypothetical situation of an infinitely dense mesh of infinitesimal elements, the error due to the FEM method tends to zero. It must be noted that these are no longer finite elements and that this situation is entirely impractical to solve.

Due to the high number of calculations required for an accurate solution, FEM is generally done using computers. Solving across denser meshes takes more time and requires more memory. Many different algorithms for FEM evaluation exist which attempt to

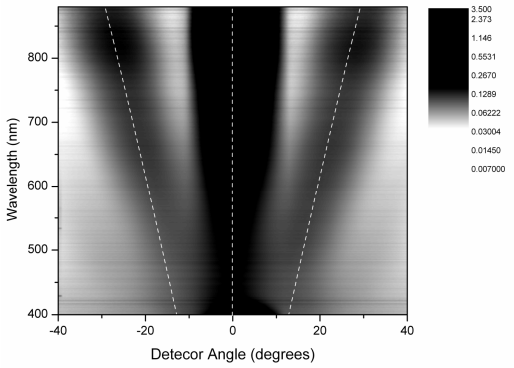

Figure 3: Colour-scale plot showing the mean measured optical transmission data taken using a white light illuminant and collected from the valves of 5 separate diatoms. The solid black lines represent the theoretically predicted zero and first order diffraction modes.

improve efficiency for systems with certain properties or symmetries. One class of solvers worth mentioning are iterative solvers, which work by repeatedly improving on or refining an approximate first solution. This can reduce memory requirement at the cost of time.

Alternative to Finite Element methods are analytical methods. Though often faster, analytical modelling is limited to regular structures, and quickly becomes inefficient if irregularities are introduced. Analytical and Finite Element methods may be combined, as in boundary element methods, wherein homogeneous regions of a structure may be solved analytically, while the boundaries between them are discretised using a finite element basis. The analysis employed here uses FEM to solve problems involving electromagnetic waves travelling in diatom-like dielectric structures.

B. Techniques and Methods

All FEM modelling used here was performed using COMSOL[28], a commercially available finite element analysis software package. The structures studied were modelled by defining the dielectric constant, ε as a function of position, r, within a finite region. The region is then discretised to give the mesh of finite elements. In some cases, 'adaptive mesh refinement' was used. This is a method of improving solution accuracy by adapting the mesh to the problem's physical behaviour[29].

The incident fields are defined as plane waves. Thus for an transverse electric wave propagating in the y-direction, the incident field is as follows: $E_{0z} = e^{-ik0ny}$. Finally, the problem is solved to discover the form of the electric and magnetic fields in the structure and the solution stored to disk. Using the data for the electric field $\boldsymbol{E}$ and magnetic field $\boldsymbol{H}$, the power can be calculated at any point within the mesh using the Poynting vector. COMSOL allows the model to be solved in such a way that incident and scattered fields can be treated separately in post processing.

Integrating the Poynting vector magnitude for incident and scattered fields along boundaries positioned above and below the structure allow the calculation of R and T; the total reflected and transmitted power. It is then possible to normalize these values using the incident power along these boundaries, so that: $R + T = 1$. Since none of the models studied include any form of optical absorption or emission by the structures, any deviation from this condition can be regarded as erroneous, with any deviation from the value, $R + T = 1$ indicating of the magnitude of the error.

For calculations with varying parameters such as frequency or angle, a parametric solver was used to increment a given parameter before resolving the problem. Many of the problems were solved using scripts written to avoid performing repetitive actions manually and to access various parameters more easily than is possible using the user interface.

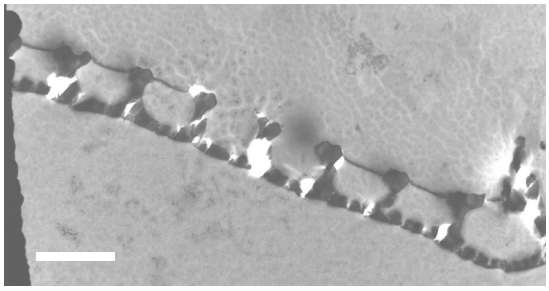

Figure 4: Transmission electron micrograph image showing a cross-section through the frustule of a typical *C. wailesii* diatom. [Scale bar: 2 μm].

C. Comparisons with analytical solutions

In order to evaluate the physical significance of the results of the FEM simulations, simple, regular structures were also modelled using the same techniques, and the results compared with analytical calculations for these structures. The thin film analysis software package, TFCalc[30] was used for analytical calculations. The basic model was created as a two-dimensional unit cell, periodic in the x-direction, with perfectly matched layers (PML) above and below the structure in the y-direction. Perfectly matched layers are designed to absorb outgoing radiation without reflection, allowing the computational region to be truncated without introducing further interfaces to the model. This arrangement was tested by simulation of reflection and transmission from a simple slab or thin film as a function of wavelength at normal incidence.

The resultant spectra compare favourably with analytical calculations using Fresnel's equations. At short wavelengths, the FEM calculations were seen to be less accurate. This is to be expected, as such a wave will have fewer mesh nodes within one period and so is not well approximated. Refinement of the mesh reduces this inaccuracy, with a sufficiently dense mesh providing a solution that converges to the analytical one.

Comparisons were also made with Fresnel's equations for reflection and transmission as a function of angle of incidence for a constant wavelength. The FEM simulation resulted in a reasonable approximation close to normal incidence.

However, taking $R + T = 1$ as an indication of the

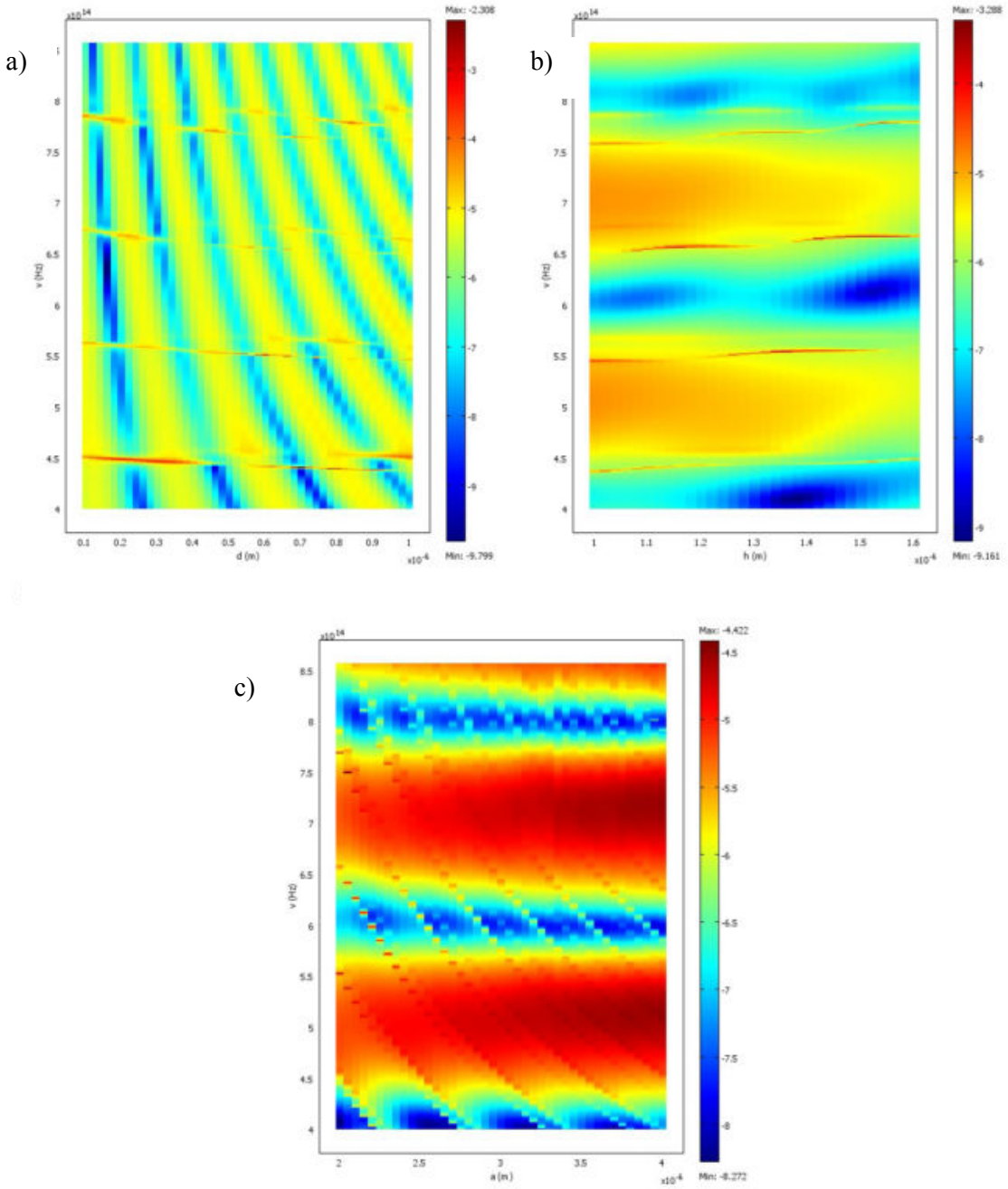

Figure 5: Colour maps showing the variation of reflectance, R as a function of the dimensions of the single layer structure and as a function of frequency, ν. (a) log(R) as a function of ν and slab thickness, d; (b) log(R) as a function of ν and hole diameter, h; and (c) log(R) as a function of ν and lattice constant, a.

error, an oscillating systematic error increasing exponentially as the angle approaches grazing incidence can be seen. This renders such simulations unreliable beyond 50◦.

D. Band Structure Calculations

A script was written to calculate band structures. The script increases the Bloch wavevector (k) in constant increments along the edge of the Brillouin zone, searching for a number of eigenvalues around a given value for each k step. Solutions, λ are stored in a matrix and a plot of ω (angular frequency of incident radiation) against k gives the band diagram. When the script was applied to the diatom model, it became clear that there was a problem with the storage of the mode data. By simply searching for eigenvalues around a fixed value, modes can 'jump' between rows in the result matrix. That is to say that if the modes of the structure increase in frequency with k then one mode may move out of range of the search at high frequency, while another comes into range at low frequency. This results in the new mode being stored in the first row of the result matrix, whereas for previous k values a different mode occupied this row. This presents difficulties in plotting the modes on a band diagram and does not allow calculations such as group velocity to be calculated.

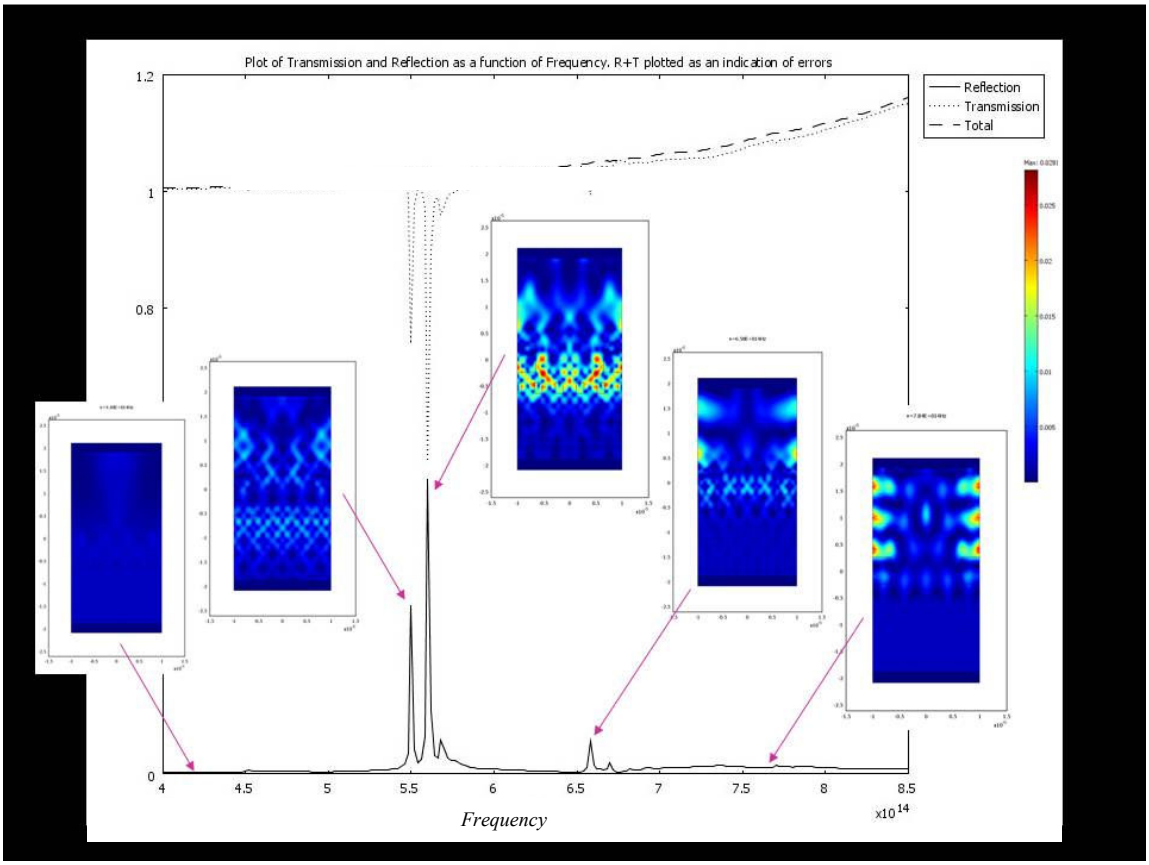

Figure 6: Theoretical reflection from the modelled double layered diatom structure at normal incidence, with plots of time-averaged normalised power for specific frequencies associated with resonant mode positions.

The solution was to adapt the script to follow the modes. The adapted script finds an initial set of eigenvalues about the centre of the frequency range studied, then each mode is followed by increasing k and taking the previous eigenvalue plus the gradient of the previous step as the eigenvalue search point. This adapted script correctly stores all modes, with distinct modes occupying their own rows in the result matrix. However, care must be taken, since modes not found in the initial ($k = 0$) search are not indexed, which can result in an incomplete band diagram.

V. Analysis of Modelling Results.

A. Modelling a single layer of the diatom structure

Initially, only the outer layer of the diatom frustules was modelled. This layer is 500 nm thick with a hexagonal array of circular holes of diameter 1300 nm with a lattice constant of 2000 nm. Reflection and transmission were calculated for normal incidence as a function of wavelength. For the thin film without holes, the reflectance fluctuates sinusoidally. However, in addition to this, a series of sharp peaks can be seen, presumably due to the periodic array of holes.

To investigate the significance of the structure's dimensions with respect to the reflection spectra, calculations were made for a range of values for each of three dimensions; the hole diameter, h, the slab thickness, d, and the lattice constant, a. Figure 5 shows the resultant colour maps. The logarithm of the reflected power is taken so that the narrow peaks of reflection do not make the comparatively weak reflected power elsewhere difficult to examine. These plots suggest that the narrow peaks and weaker broad peaks are largely separate in origin. The broad peaks depend solely on the slab thickness (figure 5(a)), while the narrow peaks are affected by the hole diameter (figure 5(b)) but more significantly by the lattice constant (figure 5(c)). Slight reductions in the height of the broad peaks as the hole diameter increases may be attributed to the reduction in length of the reflecting interface.

B. Addition of the second layer

The addition of a second layer of silica, with holes 250nm in diameter and a lattice constant of 400 nm completes the two dimensional section through the diatom frustule. Figure 6 shows reflectance as a function of frequency for this structure. In addition to the weak reflection due to the thin film effects, a repeating series of 3 modes with constant interval in frequency are observed. Examining the spatial distribution of power throughout the structure at frequencies for which reflectance peaks shows a very strong, regular arrangement of nodes and antinodes that are consistent with strong optical resonances at these frequencies. The formation of such strong

standing waves within the structure suggests that the field is resonant at these frequencies.

C. Eigenfrequency analysis and band diagrams

Eigenfrequency analysis of the diatom model in the visible frequency range yields figure 7, a band diagram showing allowed modes for transverse electric polarisation. Owing to the symmetries present in the section modelled, the band structure for TM radiation is very similar. Similar models such as 2D periodic dielectric waveguides can be seen to have similar band structures at high frequencies. However, at such frequencies it is clear that no complete band gaps exist.

Partial band gaps occurring only for a specific polarisation are not apparent either. Examining the decay constants of the various modes does show some resonant modes to be considerably stronger than others. However, since there is no competition between modes, their decay constants cannot be seen to be of great significance in the control of light within the structure. While some modes may resonate with greater intensities, they would not inhibit the propagation of other modes. Nonlinear effects were not considered and would not usually occur in the marine environment. Comparing this band structure with the results obtained earlier in this report using non-FEM modelling techniques, suggests there is no evidence for the variation in transmission of light of different wavelengths that was observed experimentally. However, it must be noted that the two dimensional model lacks many components which may be significant in producing a partial bandgap. Firstly, the 2D model is periodic in one dimension only. This limits the possibility of a bandgap to a single axis, since the structure is finite in width. Furthermore, the model lacks the six-fold symmetry of the hole array on the outer layer. It must also be noted that the dielectric contrast between seawater (n = 1.33) and amorphous silica (n = 1.5) is considerably less than in most structures exhibiting complete bandgaps. Although bandgaps may exist for any $n_1/n_2 \neq 1$, the closer the ratio is to one, the smaller the bandgap magnitude.

To examine the effect of the supposed band structure on reflectance, the reflection spectrum was calculated for a range of incident angles. Varying the angle of incidence changes the *x*-component of the wavevector, since $k_x = k_0 \sin\theta$ and so a parallel may be drawn with the band diagram. However, the two do differ. The band diagram represents the frequencies which can propagate within the structure without decaying, as a function of a wavevector in the direction of the periodicity. The reflection data as a function of angle does not directly consider the modes that can propagate, but rather their effects on the transmission of power by the structure. The *y*-component of the wavevector will also affect which modes are established, since the fields may be scattered at an arbitrary angle at the interfaces. This means that for a given frequency, modes associated with the corresponding wavevector magnitude, k_0 can always exist, independent of the angle of incidence. As such, this plot is more likely to show effects

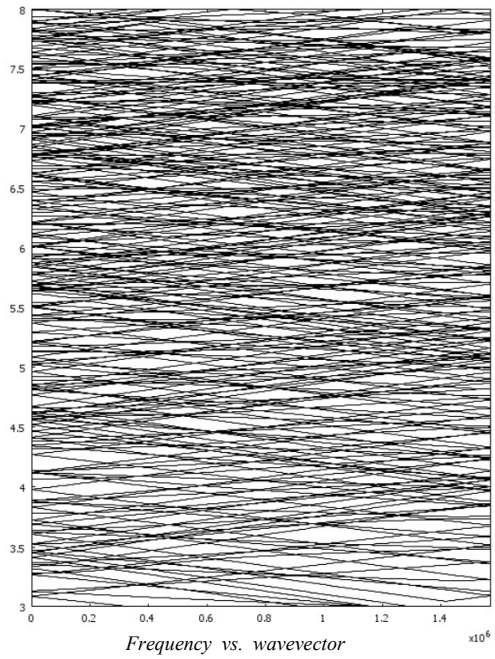

Figure 7: Theoretical band structure of diatom model for visible frequency range, TE polarised incident light.

caused by combinations of different modes and by diffraction.

Figure 8 is a logarithmic plot of reflectance as a function of frequency and angle of incidence. The logarithm is taken to allow for the extremely large reflection values calculated at high angles. It must be remembered that at these angles the errors are extremely large and the data is included only for completeness.

The peaks of reflectance seen in figure 6 can be seen to remain constant in frequency at all angles, with slight fluctuations in intensity. While narrow, these repeating modes almost certainly owe their existence to the periodicity of the structure. As such, they may be regarded as partial photonic bandgaps. However, they cannot be matched to the partial band gaps observed experimentally in this project as they occur more or less uniformly throughout the visible range and no significant difference between reflection of red, green and blue wavelengths can be seen.

Band structure analysis provides a concise and very complete description of a photonic structure's properties. However, in the case of the 2D diatom section, the lack of bandgaps in the frequency range studied means that the model could in many ways be better regarded as a diffraction grating than a photonic crystal. It could therefore be argued that analysis of transmitted and reflected power using the Poynting vector is more appropriate, as the structure clearly does not possess a small number of well defined modes which could be understood by a band diagram. It must nevertheless be remembered that the comparison with Fresnel's equations showed the finite element model to produce large errors at high angles of incidence, rendering the transmission and reflection data unreliable beyond about 50◦.

D. Summary of Modelling.

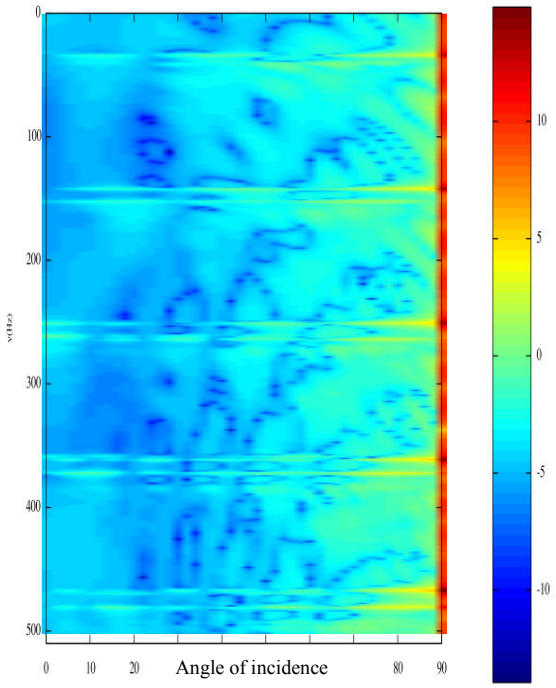

Figure 8: Theoretical log(*R*) as a function of incident angle and frequency for the modelled diatom structure.

The photonic properties of the diatom *C. wailesii* may benefit it by improving light distribution within the organism, thus preventing bleaching of chloroplasts under intense sunlight. However, the modelling completed here so far has shown that in the 2D case, the low dielectric contrast between silica and sea water means such control over the propagation of light may well be confined to narrow wavelength bands, and does not amount to a complete band gap for any visible radiation. It is possible that modelling the diatom's nanostructures in 3D or modelling a 2D section parallel to the surface would give greater insight into their photonic properties. However, from the perspective of this very preliminary FEM modelling, it is not possible to confirm that the specific resonant photonic modes discovered by the FEM model are necessarily useful to the diatom. Much more detailed follow-up fully 3D FEM modelling is necessary to understand these diatom structures from a theoretical light manipulation perspective.

VI. Discussion

Previous theoretical modelling of centric diatom ultrastructure has suggested that specific bands of incident light can efficiently couple into guided modes in the diatom valve shell walls[19]. These waveguide-coupled wavelength bands are complementary to light that is transmitted through the valve shell walls and into the interior of the diatom and this creates a strong wavelength-dependence associated with that transmitted light[19]. The existence of this wavelength dependence has been confirmed here by quantitative experiments. The results, shown in figure 2 for single *C. wailesii* valves, reveal greater than a 350% and 250% difference between the transmitted red wavelengths compared to blue and green wavelengths respectively, under the normal incidence illumination conditions described. Approximately 80% of red light (specifically λ = 633nm) was measured in transmission through the valve shell walls. While the majority of the remaining 20% of red light was reflected from the valve surface, a significantly smaller proportion (<5%) is unaccounted for within the extensive solid angle over which both transmission and reflection were collected. We suggest this light may be coupled, albeit inefficiently, into shell wall guided modes, subsequently emerging outside the collection angle. Previous theory, based on perfectly periodic valve ultrastructures, predicted guided modes at highly specific wavelength bands. However, the results here for red light suggest that the small deviation from perfect periodicity, which is inherent in these real valve ultrastructures, leads to weak coupling conditions outside the theoretically predicted[19] guided mode wavelength range.

The spatial diffraction pattern associated with the passage of light though the valve ultrastructure, although predictable from the symmetry of the ultrastructure, is experimentally confirmed here. Of the two shell walls of the valve, it is the inner shell wall comprising the larger spatial periodicity that contributes most significantly to the observed diffraction patterns. The outer shell wall, that comprises much smaller spatial periodicity, is non-diffracting at visible wavelengths and normal incidence.

From a biological perspective, it is interesting to try to interpret this experimentally-measured interaction of light with the *C. wailesii* valve ultrastructure. To do so, it is important to appreciate that solar conversion efficiency and photosynthetic productivity are among the most important processes in diatoms. They are archetypal aquatic photobiological organisms that need to capitalise on available radiant energy so that their internally located chloroplasts may harvest light efficiently for photosynthesis. For this purpose, large arrays of optically absorbing pigments are assembled for efficient light harvesting within diatoms' chloroplasts[31]. These pigments are usually chlorophyll–protein molecular complexes called biological antennas[32]. Their function is to gather electromagnetic energy over a large 3D absorption cross-section and to direct the absorbed energy to the photosynthesis reaction centres[33]. An additional detail involving the interaction of light with the chloroplasts themselves is that in some diatom species, there is evidence of chloroplast phototactivity; they have been observed congregating close to the cell walls under low light conditions, and move away from the walls when the illumination becomes more intense[11,34]. The mechanism for this is not well understood. There is also the variable associated with the range of water depths, from zero to many metres, between which centric diatoms like *C. wailesii* appear to cycle[35]. Wavelength-dependent optical attenuation of water will complicate any interpretation of light interaction still further.

Purely from the perspective of the optical data presented here, however, one might argue that energy delivery to the chloroplasts may potentially occur in two ways. If the chloroplasts closely line the cell walls, as they appear to in some species under dim lighting conditions, they will be well within the evanescently decaying fields associated with the strongly coupled optical waveguide modes[19]. This would provide access to the incident electromagnetic energy linked to the poorly transmitted light (associated with blue and green spectral bands for *C. wailesii* in this study). However, since the penetration depth of this decaying field is of the order of no more than a few tens of micrometers, this would cease to supply the chloroplasts energy needs in the same way when they moved away from the cell walls.

Conversely, however, whether the chloroplasts are close to or relatively distant from the cell walls, they will continuously be in the near- or the far-field of the strongly transmitted diffracted light (the red spectral band for *C. wailesii*). It may be argued that this would provide a more constant source of long-wavelength energy which is much more independent of lighting conditions close to the water surface. It might also be argued that the strong diffraction exhibited by this long-wavelength light passing through the diatom valve, identified in these experiments, is a mechanism by which this energy is spatially distributed more evenly over the internal volume of *C. wailesii* (figures 2e and 2f). This potentially creates a relatively more constant field of illumination inside the diatom for efficient light collection by a much larger number of chloroplasts located throughout its interior. It would also potentially minimise the likelihood of photobleaching-related damage under very intense illumination in any one unit volume of the diatom, especially for chloroplasts near light-incident surfaces. This aspect should be considered because evidence indicates that very intense optical fields cause damage arising from permanent photoreceptor bleaching due to excessive light collection by the photosynthetic antennae[36,37].

Growth optimisation dynamics associated with diatoms' biominerlisation processes have previously been described as one of the reasons for their observed highly periodic ultrastructures[12]. Other reasons have been ascribed to nutrient status control[38], hydrodynamic control[39] and even mechanical strengthening for protection from predation[40]. It is not yet possible to conclude whether the photonic effects generated by the *C. wailesii* ultrastructure are a further reason for its development into such highly periodic forms. Certainly, the experiments described here show that the extent of light manipulation offered by its ultrastructure is significant. More detailed and specific work is underway to investigate specifically whether there is an adapted optical benefit for *C. wailesii* and other centric diatoms from the way in which their ultrastructure interacts with incident light.

There is keen interest from materials chemists, biologists and technologists in exploiting diatoms for applications. The experimental results presented in this study are relevant to those applications which comprise optical themes or components, for instance; incorporation of fluorescent material in or on the diatom for sensing-related applications[1,4], or the use of photoluminescence or electroluminescence effects associated with diatoms that have had their surface or bulk chemistry altered by design[41]. For fluorescence applications, efficient light delivery to an appropriate diatom region is necessary for efficient subsequent fluorescent excitation. The experimental data for light delivery to the interior of *C. wailesii* presented here, should aid in the choice or design of the fluorescent species considered for encapsulation inside it and for interpretation of the fluorescent light emerging from it. Alternatively, the choice of materials to be engineered or biomineralized into diatomaceous cell walls for specialised luminescence purposes should be guided by the nature of the electric fields associated with the efficiently coupled guided modes that appear excited within the cell wall structures.

It may be debatable to refer to diatoms strictly as being photonic crystals. However, the results of this investigation of a representative centric diatom species indicate its cell walls significantly manipulate the flow of light, in air or in water, due to the scale and geometry of its ultrastructure. We suggest that the character of this light manipulation should be considered in the conception and design of biomimetic optics-based diatom applications.

References

1. F.E. Round, R.M. Crawford, and D.G. Mann, *The Diatoms: Biology and Morphology of the Genera* (Cambridge Univ. Press, Cambridge, UK, 1990).
2. C. Sanchez et al., Biomimetism and bioinspiration as tools for the design of innovative materials and systems, *Nature Materials*. **4**. 277-288 (2005).
3. P.J. Lopez et al., Prospects in diatom research, *Current opinion in Biotech*. **16**, 180-186, (2005).
4. J. Parkinson and R. Gordon. Beyond micromachining: the potential of diatoms. *TIBTECH*, **17**, 190-196, (19 99).
5. S.H. Liu, C. Jeffryes, G.L. Rorrer, C.H. Chang, J. Jiao, and T. Gutu, Blue Luminescent Biogenic Silicon-Germanium Oxide Nanocomposites, 2005, in *Biological and Bio-Inspired Materials and Devices,* edited by K.H. Sandhage, S. Yang, E. DiMasi, *Mater. Res. Soc. Symp. Proc.* Vol. 873E, Warrendale, PA, K1.4.1-K1.4.6.
6. U. Kusari, Z. Bao, Y. Cai, G. Ahmad, K.H. Sandhage and L. G.Sneddon, Formation of nanostructured, nanocrystalline boron nitride microparticles with diatom-derived 3-D shapes, *Chem. Comm*, 1177–1179, (2007).
7. Z. Bao, et al., Chemical reduction of three-dimensional silica micro-assemblies into microporous silicon replicas. *Nature*. **446**, 8, 172-175, (2007).
8. L. De Stefano, et al. Interfacing the nanostructured biosilica microshells of the marine

diatom *Coscinodiscus wailesii* with biological matter., *Acta Biomaterialia*. **4**, 126-130, (2008).

9. R.R. Naik and M.O. Stone. Integrating biomimetics. *Mat. Today*. **8**, 18–26, (2005).

10. D. Losic, et al., Controlled pore structure modification of diatoms by atomic layer deposition of TiO_2, *J. Mat. Chemistry*, **16**, 4029-4034, (2006).

11. M. Sumper and E. Brunner. Learning from diatoms: Nature's tools for the production of nanostructured silica, *Adv. Funct. Mater*., **16**, 17-26, (2006).

12. M.Sumper. A phase separation model for the nanopatterning of diatom biosilica, , *Science,* **295**, 2430-2433, (2002).

13. M. Srinivasarao. Nano-Optics in the Biological World: Beetles, Butterflies, Birds, and Moths, *Chem. Rev*. ***99***, 1935 – 1962, (1999).

14. P. Vukusic and J.R. Sambles. Photonic structures in Biology, *Nature* **424**, 852-855, (2003).

15. S. Kinoshita and S. Yoshioka, eds., *Structural Colors in Biological Systems: Principles and Applications* (Osaka Univ. Press, Osaka, 2005).

16. M. Gale, Diffraction, beauty and commerce. *Physics World*, **2**, 24–28, (1989).

17. P. Vukusic. Natural Photonics, *Physics World*, **17**, 35-39, (2004).

18. Hutley M.C., *Diffraction Gratings* (Academic Press, New York, 1982).

19. T. Fuhrmann, S. Landwehr, M. El Rharbi-Kucki and M. Sumper, Diatoms as living photonic crystals, , Appl. Phys. B., **78**, 257-260, (2004).

20. Z. Dubinsky, P.G. Falkowski and K. Wyman. Light Harvesting and Utilization by Phytoplankton, *Plant Cell Physiol.* **27**, 1335-1349, (1986).

21. P. Vukusic, J.R.Sambles, C. R. Lawrence and R.J. Wootton, Quantified interference and diffraction in single *Morpho* butterfly scales, *Proc. R. Soc. London Ser.* B., **266**, 1403-1411, (1999).

22. I. Hooper and P. Vukusic, , Detailed optical study of the transparent wing membranes of the dragonfly *Aeshna cyanea*, *Optics Express*, **14**, 4891-4897, (2006).

23. J.A. Noyes, P. Vukusic and I.R. Hooper, Experimental method for reliably establishing the refractive index of buprestid beetle exocuticle, *Optics Express*, **15**, 4351-4358, (2007).

24. E. Abbe, Beiträge zur Theorie des Mikroskops und der mikroskopischen Wahrnehmung, *Schultzes Arc. f. Mikr. Anat.* **9**, 413–468, (1873).

25. S.D. Wilson, , A reflection-diffraction microscope for observing diatoms in colour, *App. Optics*, **5**, 10, 1683-1684, (1966).

26. F.A.S. Sterrenburg. Studies on the genera *Gyrosigma* and *Pleurosigma*. Light microscopical criteria for Taxonomy. *Diatom Research,* **6**, 367-389, (1991).

27. C.Kittel, *Introduction to Solid State Physics* (John Wiley and Sons, London, 1995).

28. www.comsol.com

29.www.comsol.com/products/multiphysics/glossary/

30. www.sspectra.com/

31. A. Falciatore and C. Bowler. Revealing the Molecular Secrets of Marine Diatoms, , *Ann. Rev. Plant Biol. **53**, 109–30,* (2002).

32. W. Foster and R.D. Smyth, Light Antennas in phototactic algae, *Microbiol Rev*., **44**, 572–630, (1980).

33. P. Horton, A.V. Ruben and R.G. Walters, Regulation of light harvesting in green plants, *Annu Rev Plant Physiol Plant Mol Biol.* **47**, 655–684, (1996).

34. T. Furukawa, M. Watanabe and I. Shihira-Ishikawa, Green- and blue-light-mediated chloroplast migration in the centric diatom *Pleurosira laevis*) provides insight into their adapted survival strategy in conditions of variable light, *Protoplasma*, **203**, 214-220, (1998).

35. O. Akira, I. Kazuhiko and T. Kuninaho, The Standing Stock and Sinking Rate of the Large Diatom *Coscinodiscus wailesii* Causing Nori (Porphyra) Discoloration, *Bull. Soc. Sea Water Science, Japan*, **60**, 253-259 (2006).

36. A.R. Grossman, D. Bhaya, K.E. Apt and D.M.Kehoe, Light-Harvesting Complexes in Oxygenic Photosynthesis. *Diversity, Control, and Evolution Annual Review of Genetics*, **29**, 231-288, (1995).

37. M. Neumüller, A. Cunningham and D. Mckee, Assessment of a microscopic photobleaching technique for measuring the spectral absorption efficiency of individual phytoplankton cells, *J. Plankton Res*. **24,** 741-746, (2002).

38. D. Tilman and P. Kilham, Sinking in freshwater phytoplankton: Some ecological implications of cell nutrient status and physical mixing processes. *Limnol. Oceanogr.* **21**, 409-417, (1976).

39. M.S. Hale, and J.G. Mitchell, , Functional morphology of diatom frustule microstructures: hydrodynamic control of Brownian particle diffusion and advection, , *Aquat. Microb. Ecol*. **24**, 287-295, (2001).

40. C.E. Hamm, R. Merkel, O. Springer, P. Jurkojc, C. Maier, K. Prechtel and V. Smetacek, Architecture and material properties of diatom shells provide effective mechanical protection, *Nature,* **421**, 841-843, (2003).

41. A.R. Parker and H.E. Townley, Biomimetics of photonic nanostructures, *Nature Nanotech.* **2**, 347 – 353, (2007).